Proceedings of the Optical Society of Korea Annual Meeting 2001 (2001. 2. 15~16)

Atomic-scale Controlled Epitaxial Growth and Characterization of Oxide Thin Films

G.Z. Yang*, H.B. Lu, F. Chen, T. Zhao, Z.H. Chen
Laboratory of Optical Physics, Institute of Physics, Center for Condensed Matter Physics, Chinese Academy of Sciences, Beijing, 100080, China

ABSTRACT

More than ten kinds of oxide thin films and their heterostructure have been successfully fabricated on $SrTiO_3$ (001) substrates by laser molecular beam epitaxy (laser MBE). Measurements of atomic force microscopy (AFM), high-resolution transmission electron microscopy (HRTEM) and X-ray small-angle reflectivity reveal that the surfaces and interfaces are atom-level-smooth. The unit cell layers and the lattice structure are perfect. The electrical and optical properties of $BaTiO_{3-X}$ thin films and $BaTiO_3/SrTiO_3$ (BTO/STO) superlattices were examined. The all-perovskite oxide P-N junctions have been successfully fabricated and the better I-V curves were observed.

1. INTRODUCTION

Oxide materials have attracted much attention because of their various properties : insulating, ferroelectric, ferromagnetic, superconducting , semiconductive, and others. Since the discovery of high Tc superconductors, enormous efforts have been devoted to the epitaxial growth of oxide thin films. Various techniques have been applied to form oxide films. The fabrication of artificial crystalline materials through layer-by-layer epitaxial growth with full control over the composition and structure at the atomic level has become one of the most exciting areas of research in condensed matter physics and materials sciences.

Laser molecular beam epitaxy (laser MBE) uses the both merits of pulsed laser deposition and conventional MBE for depositing films, especially for high melting point ceramics and multicomponent solids, controlled in atomic scale[1-3]. Laser MBE has attracted much on the interest in recent years as a promising new technology for opening a new field of oxide-based electronics. The current status of this advanced laser processing technology is presented with a focus on its significance for exploiting quantum structures and properties of oxides. In this letter, we report the epitaxial growth and characterization of perovskite oxide thin films. We have observed more than 1000 cycles of intensity oscillation during the epitaxial growth of oxide thin films by a in-situ reflection high-energy electron diffraction (RHEED). Measurements of atomic force microscopy (AFM) and high-resolution transmission electron microscopy (HRTEM) reveal that the surfaces and interfaces of the oxide films and superlattices are atomically smooth. The lattice structures of the films and superlattices are perfect. The electrical and optical properties of $BaTiO_{3-X}$ thin films and $BaTiO_3/SrTiO_3$ (BTO/STO) superlattices were examined.The all-perovskite oxide P-N junctions have been successfully fabricated and better I-V curves were observed.

2. ATOMIC-SCALE CONTROLLED EPITAXIAL GROWTH

. The computer-controlled laser MBE system we used is composed of four main parts: (1) an ultra-high vacuum (UHV) epitaxial chamber with a background pressure $1.3x10^{-8}$ Pa containing a four-target holder and a substrate holder, (2) a XeCl excimer laser with a wavelength 308 nm, (3) composition scanning device of the laser beam and the target, and (4) a RHEED system and charge coupled device (CCD) camera [4]. The in situ RHEED and CCD camera can provide us with useful information on the crystal structure and morphology of a

* Correspondence: Email: gzyang@aphy.iphy.ca.cn, Fax: 86-010-82649531

growing film surface. The RHEED intensity oscillation enables us to control the exact number of grown molecular layers.

Before deposition, the substrate was annealed at 630^0C for 20-30 min under 1×10^{-4} Pa O_2 to clean up the surface of the substrate. Then about 20 unit cells of homoepitaxial $SrTiO_3$(STO) were first grown on the substrate to improve the surface smoothness. We can observe more than 1000 cycles of RHEED intensity oscillations during the epitaxial growth of oxide thin films. Fig.1 shows a part of a RHEED intensity oscillation monitored on the specular beam spot during the growth of a homoepitaxial STO film. Fig.2 shows the change of RHEED oscillation intensity during the growth of a STO/BTO superlattice with the stacking combination of 10 unit cells/ 10 unit cells. We can always observe the fine streaky patterns and undamped RHEED intensity oscillation during the epitaxial growth. STO, BTO, $LaAlO_3$, $SrVO_3$, $SrMoO_3$, $LaTiO_3$, ZrO_2, MgO and others, more than ten kinds of oxide thin films and their heterostructures have been successfully fabricated on STO(001) substrates by the laser MBE.

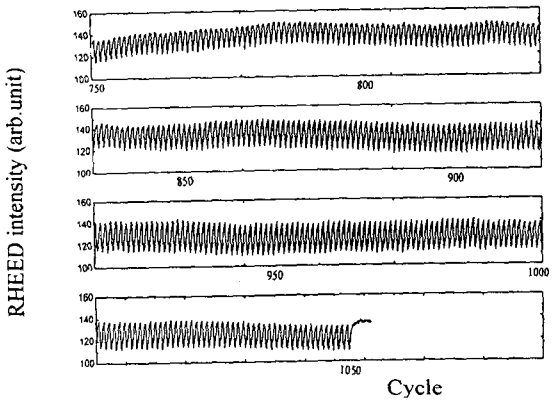

Fig.1 A part RHEED intensity oscillation of STO homoepitaxy (the oscillation cycle from 750 to 1050).

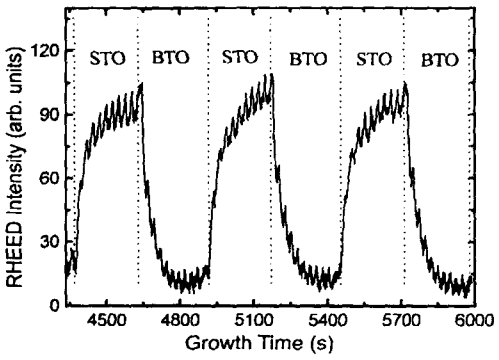

Fig.2 RHEED intensity oscillations of the epitaxy of BTO(10 unit cells)/STO(10 unit cells) .superlattice

3. MICROSTRUCTURE AND MORPHOLOGY

3.1. BTO and STO Ultra-thin Films.

BTO and STO ultra thin films of 1 to 10 unit cell layers have been successfully fabricated on STO (001) substrates by the laser MBE.[5] The surface morphologies of the BTO and STO ultra thin films were examined by atomic force microscopy (AFM) equipped in a UHV chamber. Fig.3 (a) shows a typical two-dimension (2D) AFM image of 3 unit cells (12Å) BTO thin film on STO substrate, and Fig.3 (b) is the height profile along the diagonal of the 2D image in Fig.3 (a). The root-mean-square (rms.) surface roughness is 0.55Å in 1μm×1μm.

Fig.4 (a), (b) and (c) show the cross sectional HRTEM lattice images of 1, 2 and 3 unit cell layers BTO thin films on STO substrates, respectively. The perfect unit cell layers and the lattice structure can be seen on the images. The BTO ultra thin films of unit cell layers have high degree of c-axis-oriented epitaxial crystalline structure.

The BTO and STO ultra thin multilayers films were fabricated by the laser MBE. The layer thicknesses and the roughnesses of surfaces and interfaces were examined by X-ray small-angle reflectivity which is a powerful method to determine the layer thickness and roughness of surface and interface.[6] Fig.5 (a) and (b) show the X-ray small-angle reflectivity curves for sample A and sample B. The solid curves are theoretical curves to fit the experimental data. The calculated results of reflectivity show the layer thickness of BTO and STO are (12±1) Å and (8±1)Å for sample A, (11±1)Å and (12±1) Å for sample B, respectively,

which are in excellent agreement with the results obtained from RHEED intensity oscillation. The roughness of the surfaces and interfaces of the two samples are about 2Å, indicating that the BTO and STO layers have atom-level-smooth surfaces and interfaces.

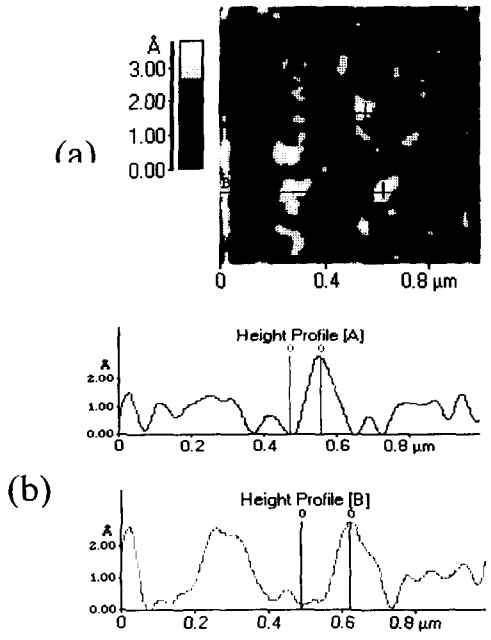

Fig.3 AFM image: (a) 2D image (1μm×1μm) of BTO (12Å)/STO, and (b) the height profile along the diagonal of the 2D image (a).

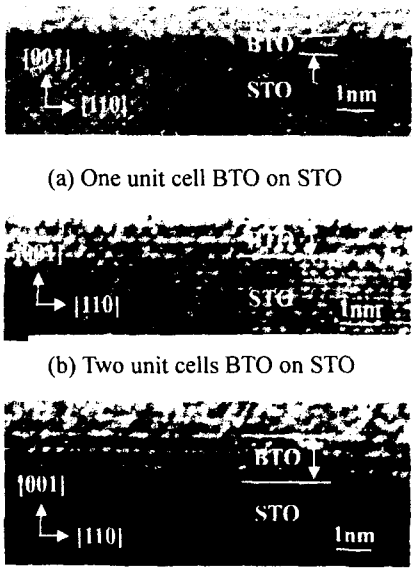

(a) One unit cell BTO on STO

(b) Two unit cells BTO on STO

(c) Three unit cells BTO on STO

Fig.4 Cross-sectional HRTEM images Of ultra-thin films.

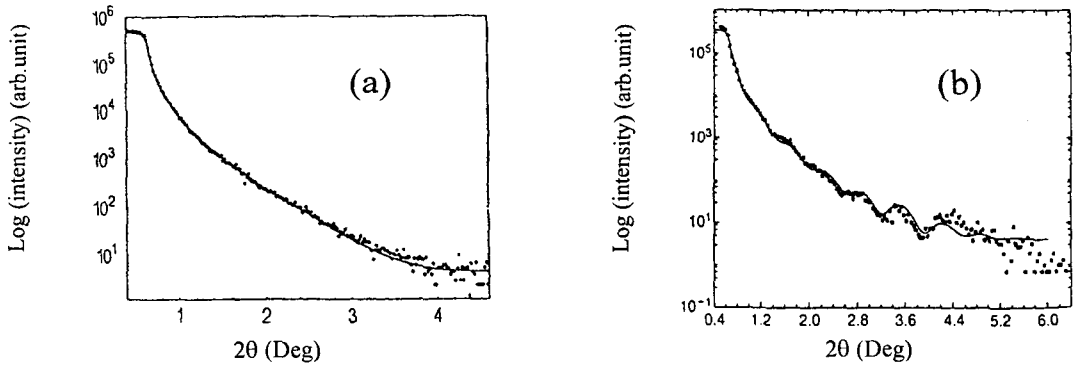

Fig.5 The X-ray small-angle reflectivity: (•) experimental data; (-) theoretical curve: (a) sample A: STO(8Å)/BTO(12Å)/STO; (b) sample B: 6× [BTO(12Å)/STO(12Å)]/STO

3.2. BTO/STO Superlattices.

A series of BTO/STO superlattices with various stacking periodicities were fabricated by laser MBE. The thickness of each BTO or STO layer was varied in the range from 8Å (2 unit cells) to 200Å (50 unit cells) and the total thickness of the superlattices were about 800Å. The surface morphology of the BTO/STO superlattices was examined by AFM. According to our observations, the surface of the BTO/STO superlattices is atomically smooth and no particles have been found. The root-mean-square surface roughness is 1.01Å in an area of 20 μm ×20 μm.

The microstructure of the BTO/STO superlattices has been investigated by HRTEM (Philips CM200FEG). Fig.6 shows a typical cross-sectional HRTEM structural image of the

top-most three layers of the BTO(80Å)/STO(40Å) superlattice. As can be seen clearly, the BTO and STO lattice structures perfectly match. The number of unit cells in the BTO and STO layers are 20 and 10, respectively. The number of unit cells in the BTO and STO layers (obtained from the HRTEM image) is in excellent agreement with that calculated from the digitized by RHEED oscillation periods as recorded during the epitaxial growth. The interfaces of BTO/STO are very clear and no interfacial reaction layer is observed in the image, i.e., there is no obvious interdiffusion at the interface. The BTO/STO multilayers are perfectly oriented and the epitaxial crystalline structure shows the orientation relations of BTO (001)//STO(001) and BTO[100]//STO[100].[7]

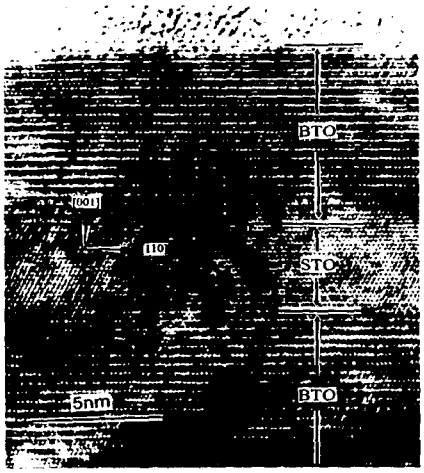

Fig.6 Cross-sectional HRTEM image of BTO(80Å)/STO(40Å) Superlattice with a total thickness of 840Å.

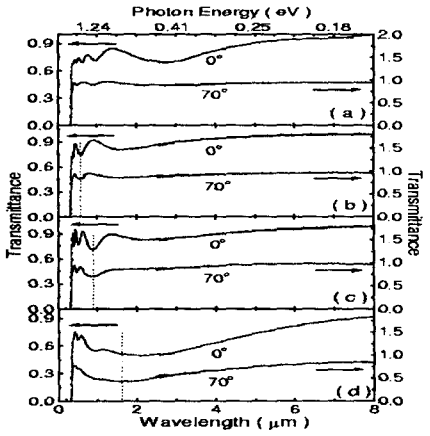

Fig.7 The optical transmittance spectra with two incident angles of 0^0 and 70^0 for (a) $BaTiO_3$, (b) $BaTiO_{2.93}$, (c) $BaTiO_{2.28}$, (d) $BaTiO_{2.52}$ thin films. The dotted lines indicate the positions of the optical absorption peaks.

4. OPTICAL AND ELECTRICAL PROPERTIES

4.1 Electrical and Optical Properties of $BaTiO_{3-x}$ Thin Films

A series of $BaTiO_{3-x}$ thin films were epitaxially grown on $SrTiO_3$ (*100*) and MgO (*100*) substrates by laser MBE under various oxygen pressures from 2×10^{-2}Pa to 2×10^{-5}Pa. The films deposited on MgO were used for optical measurements, while those on $SrTiO_3$ for other ones. The thickness of each film was 400nm.

The oxygen content in the deposited $BaTiO_{3-x}$ thin films were analyzed by Rutherford backscattering spectrometry (RBS) with an incident $^4He^+$ (3.016MeV in energy) ion beam which has been proven to be effective to detect oxygen. The results of RBS show x are 0, 0.07, 0.18, and 0.48 for the oxygen pressures 2×10^{-2}Pa, 2×10^{-3}Pa, 2×10^{-4}Pa and 2×10^{-5}Pa, respectively. The XRD measurements confirm that each of the deposited $BaTiO_{3-x}$ thin films is *c*-axis oriented tetragonal single crystal. The results show that tetragonal perovskite structure can be maintained even in the strongly reduced $BaTiO_{2.52}$ sample, which may be due to the stabilization of the tetragonality by the large misfit strain in $BaTiO_{3-x}$ thin films.

The resistivity (ρ) of the $BaTiO_{3-x}$ thin films at room temperature was measured by van der Pauw method. The resistivity ρ are 1.3×10^{10} Ωcm, 1.2×10^{7} Ωcm, 1.7×10^{-2} Ωcm, and 6.0×10^{-5} Ωcm for $BaTiO_3$, $BaTiO_{2.93}$, $BaTiO_{2.82}$, and $BaTiO_{2.52}$, respectively. With decreasing the oxygen pressure, the resistivity decreases. The variation of the resistivity is more than 15 orders of magnitude among the four $BaTiO_{3-x}$ thin films. The $BaTiO_{3-x}$ thin film changes from an insulator to a conductor. The results clearly show that $BaTiO_{3-x}$ can become highly conductive with the conductivity being much higher than what has been known so far

The optical transmittance of the four $BaTiO_{3-x}$ thin films were measured from 0.2μm to 8μm. To identify the optical absorption peak from the fringe patterns which are the characteristics in the optical spectra of thin films, two transmittance spectra with different incident angles (0° and 70°) were measured for each film. The position of the peaks originated from interference will change with varying the incident angle, while those from optical absorption will keep in same values. The optical spectra for the four $BaTiO_{3-x}$ thin films are shown in Figs.7(a) to 3(d). There isn't any absorption in the stoichiometric $BaTiO_3$ film (Fig.7(a)) besides the band edge absorption of $BaTiO_3$. For the other three oxygen deficient films, there appears a new absorption peak besides the band edge absorption. With decreasing the oxygen pressure, the peak position shifts to longer wavelength (lower energy) while the peak width becomes larger. It has been reported that optical absorption can be induced in $BaTiO_{3-x}$ by reduction[8-10]. However, the peak position reported are different from author to author. Our results clearly show that the optical absorption associate with the oxygen content and the electrical conduction. It could be reasonably assumed that the oxygen vacancies induce a doping level in the band gap of $BaTiO_3$, which makes the electrical conduction and optical absorption appear in $BaTiO_{3-x}$. The more the oxygen deficiency, the nearer the doping level to the Fermi level, and then the higher the electrical conductivity and the lower the energy of the absorption peak position would be. Moreover, oxygen deficiency makes the $BaTiO_{3-x}$ lattice be distorted, which makes the energy band expanded. Therefore, the more the oxygen deficiency, the wider the absorption peak would be.[11]

4.2 Enhancement of Second-Harmonic Generation in BTO/STO Superlattices

Second harmonic generation (SHG) of 1.064μm incident beam was investigated on BTO/STO superlattices prepared by laser molecular beam epitaxy. The incidence angle and the polarization angle dependence of the SHG coefficients were measured. The SHG coefficients were greatly enhanced by the superlattice structure with the maximum value of d_{33}=156.5pm/V being more than one order of magnitude larger than that of bulk BTO crystal.[12]

6. All-PEROVSKITE OXIDE P-N JUNCTIONS

In today's most advanced electronics research much attention is paid to the fabrication of artificially designed structures to verify new device concepts based on quantum effects. A key structure of the electronics devices is the P-N junction.

STO and BTO are perovskite metal-oxide insulator, which may be doped to yield n-type or p-type semiconductors. Dopants include Nb or In substituted on the Ti sites. The STO and BTO appear that n-type doping with Nb and p-type doping with In. The n-type $SrTi_{1-x}Nb_xO_3$, $BaTi_{1-x}Nb_xO_3$ and p-type $Sr_{1-x}In_xO_3$, $BaTi_{1-x}In_xO_3$ have been fabricated. The $SrTi_{1-x}Nb_xO_3/SrTi_{1-x}In_xO_3$, $SrTi_{1-x}Nb_xO_3/BaTi_{1-x}In_xO_3$, $SrTi_{1-x}Nb_xO_3/La_{1-x}Sr_xMnO_3$ all-perovskite oxide P-N junctions have been successfully fabricated by the laser MBE. We have observed better I-V curves. To the best of our knowledge, it is the first time to obtain the all-perovskite oxide P-N junctions. Fig.8 (a) and (b) show the I-V curves of $SrTi_{0.9}In_{0.1}O_3/SrTi_{0.99}Nb_{0.01}O_3$ and $La_{0.8}Sr_{0.2}MnO_3/SrTi_{0.99}Nb_{0.01}O_3$ P-N junctions, respectively.

7. CONCLUSION

In summary, more than ten kinds of perovskite oxide thin films and ultra thin films have been successfully fabricated on STO (001) substrates by laser MBE. The lattice structure is

perfect and the surfaces and interfaces are atom-level-smooth of the oxide thin films. They can be used for constructing artificially designed new layered lattice of oxides which may exhibit unexpected new properties or phenomena. Thus, we can explore systematically new materials and functionality in oxides. The atomic-scale controlled epitaxial growth of oxide thin films will open a door for investigating the mechanism and application of oxide.

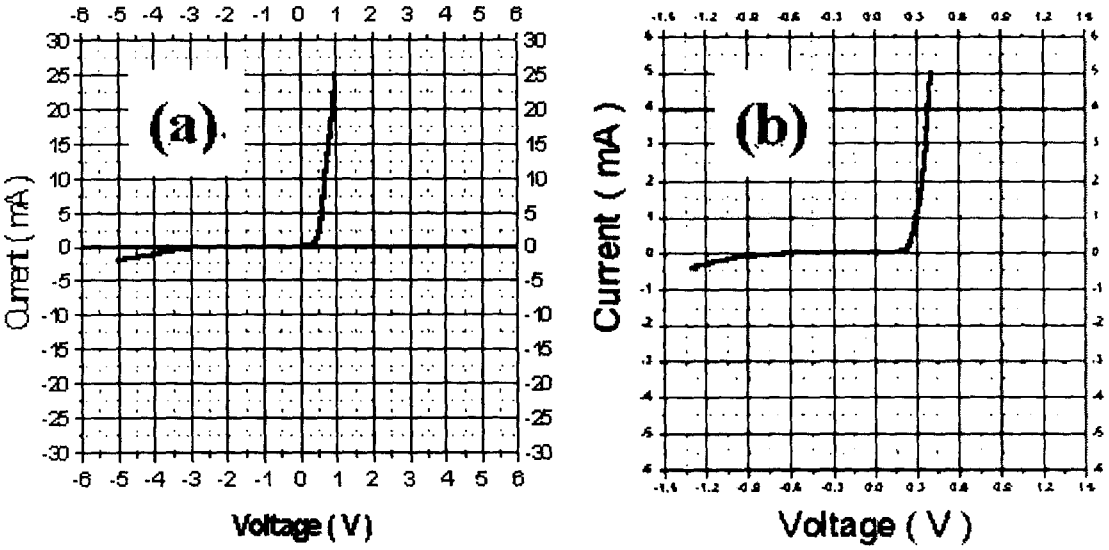

Fig.8 The I-V curves of P-N junctions (a) $SrTi_{0.9}In_{0.1}O_3/SrTi_{0.99}Nb_{0.01}O_3$ (b) $La_{0.8}Sr_{0.2}MnO_3/SrTi_{0.99}Nb_{0.01}O_3$.

ACKNOWLEDGMENTS

We thank Dr. N.Wang and Dr. A.J.Zhu for the measurements of HRTEM and X-ray small-angle reflectivity. This work were supported by a grant for State Key Program of China and National Centre for R&D on Superconductivity of China.

REFERENCES

1. M.Kanai, T.Kawai and S.Kawai, Appl. Phys. Lett. 58, 771(1991).
2. H.Koinuma, M.Yoshimoto, Appl. Surf. Sci. 75, 308(1994).
3. Yang Guozhen, Lu Huibin, Zhoy Yueliang, Lei Zhenlin, Chen Zhenghao, ACTA Physica Sinica, 7, 623(1998).
4. G.Z.Yang, H.B.Lu, Z.H.Chen, D.F.Cui, H.S.Wang, H.Q.Yang, F.Y.Miao, Y.L.Zhuo, L.Li, Science in China (A), 28, 260(1998).
5. H.B.Lu, N.Wang, W.Z.Chen, F.Chen, T.Zhao, H.Y.Peng, S.T.Lee, G.Z.Yang, J. Crystal Growth, 212, 173(2000).
6. S.F.Cui, G.M.Luo, M.Li, Z.H.Mai, Q.Cui, J.M.Zhou, X.M.Jiang, W.L.Zhang, J. Phys.: Condens. Matter, 9, 2891(1997).
7. N.Wang, H.B.Lu, W.Z.Chen, T.Zhao, F.Chen, H.Y.Peng, S.T.Lee, G.Z.Yang, Appl. Phys. Lett. 75, 3464(1999).
8. S. Ikegami and I. Ueda, J. Phys. Soc. Jpn. **19**, 159(1964).
9. C. N. Berglund and H. J. Braun, Phys. Rev. **164**, 790(1967).
10. J. Y. Chang, M. H. Garrett, H. P. Jenssen, and C. Warde, Appl. Phys. Lett. **63**, 3598(1993).
11. T.Zhao, Z.H.Chen, F.Chen, H.B.Lu, G.Z.Yang, Appl.Phys.Lett. 77, 4338(2000).
12. T.Zhao, Z.H.Chen, F.Chen, W.S.Shi, H.B.Lu, G.Z.Yang, Phys. Rev. B. 60, 1697(1999).